# Airborne observations of Arctic air mass transformations during the HALO-(AC)$^3$ campaign

**Klingebiel, M.[1], Schäfer, M.[1], Kirbus, B.[1], Maherndl, N.[1], Becker, S.[1], Brückner, M.[1], Jäkel, E.[1], Lonardi, M.[1], Luebke, A. E.[1], Maahn, M.[1], Müller, H.[1], Röttenbacher, J.[1], Schmidt, J.[1], Schwarz, A.[1], Sperzel, T. R.[1], Ehrlich, A.[1], Wendisch, M.[1]**

[1] *Leipzig Institute for Meteorology, Leipzig University, Germany*
✉*e-mail: marcus.klingebiel@uni-leipzig.de*

**Summary:** The HALO-(AC)$^3$ campaign was conducted in March and April 2022 to investigate warm air intrusions into the Arctic and marine cold air outbreaks. In coordinated flights over the Arctic, the High Altitude and Long Range Research Aircraft (HALO), equipped with a remote sensing payload and dropsondes, investigated these air mass transformations together with the research aircraft Polar 5 and Polar 6. In this report, we give an overview about the research flights and preliminary results from projects, which are carried out by employees of the Leipzig Institute for Meteorology (LIM).

**Zusammenfassung:** Die HALO-(AC)$^3$ Kampagne wurde im März und April 2022 durchgeführt, um Warmlufteinbrüche in die Arktis und marine Kaltluftausbrüche zu untersuchen. Das "High Altitude and Long Range Research Aircraft" (HALO), ausgestattet mit Instrumenten zur Fernerkundung und Standardmeteorologiesonden, untersuchte zusammen mit den Forschungsflugzeugen Polar 5 und Polar 6, in koordinierten Flügen über der Arktis, diese Veränderungen der Luftmassen. In diesem Bericht wird eine Übersicht über die durchgeführten Forschungsflüge gegeben und Forschungsprojekte werden vorgestellt, welche von Mitarbeitern des Leipziger Instituts für Meteorologie (LIM) durchgeführt werden.

## 1 Introduction

Over the last decades, the Arctic experienced an enhanced warming up to four times stronger than the mid-latitudes, which is known as Arctic amplification (Serreze and Barry, 2011; Wendisch et al., 2023; Rantanen et al., 2022). The Transregional Collaborative Research Center (TR 172) called *Arctic Amplification: Climate Relevant Atmospheric and Surface Processes, and Feedback Mechanisms* ((AC)$^3$, www.ac3-tr.de), lead by the Leipzig Institute for Meteorology (LIM), investigates the processes and key factors to get a better understanding of the causes driving the Arctic amplification. One of the suspects are general circulation patterns related to the jet stream, which might get weaker because of Arctic amplification. This results in a higher amount of blocking situations, which promote Warm Air Intrusions (WAIs) and Cold Air Outbreaks (CAOs). Such WAIs, which are most prominent in the winter time Arctic, lead to a northward

transport of moisture and clouds and, thus, increase the downward terrestrial radiation and warms the near surface air.

To understand this positive feedback mechanism and investigate air mass transformations in more detail, the HALO-(AC)$^3$ campaign was conducted in March and April 2022 to study WAIs and CAOs. The general objectives of the HALO-(AC)$^3$ mission are:

- To perform quasi-Lagrange observations of air-mass transformation processes during meridional transports with a particular focus on pronounced WAIs and marine CAOs.
- To test the ability of numerical atmospheric models to reproduce the measurements, which then can be applied to investigate the linkages between Arctic amplification and mid-latitude weather.

Extended information on the HALO-(AC)$^3$ mission are provided at the campaign webpage (HALO-(AC)$^3$ Website, 2023). Three research aircraft were involved in the campaign with different instrumentation and flight patterns, aiming at the above mentioned objectives.

The High Altitude and LOng Range (HALO) research aircraft from German Aerospace Center (DLR) is the only German research aircraft, which is capable of covering distances to up to 10000 km (10 hours flight time). For this reason, HALO is the ideal tool to perform the planned quasi-Lagrange air-mass observations. HALO is equipped with meteorological and remote sensing instruments, as well as dropsondes, to observe the complete vertical tropospheric air mass column up to an altitude of 15 km. These observations contain meteorological quantities (temperature, pressure, humidity), turbulence parameters, water vapor, aerosol particles, and clouds (HALO-(AC)$^3$ Website, 2023). During the HALO-(AC)$^3$ campaign, HALO was stationed at Kiruna, where a large hangar was available for safe and convenient aircraft operations.

The two research aircraft from the Alfred-Wegener-Institut Helmholtz Centre for Polar and Marine Research (AWI), namely Polar 5 and Polar 6, were used to study the lower atmosphere, up to 3 km. While Polar 5 was equipped with remote sensing instruments and dropsondes, Polar 6 performed in-situ measurements of cloud and aerosol particles in the boundary layer. Polar 5 and Polar 6 were stationed in Longyearbyen, Svalbard and conducted measurements in the vicinity of Svalbard. Both aircraft are specially modified to fly under extreme polar conditions and into clouds (Wesche et al., 2016).

An overview of the flight tracks from HALO, Polar 5, and Polar 6 is given in Fig. 1. As presented in Fig. 1a, HALO covers a spatial range from Kiruna towards the North Pole. Polar 5 and Polar 6 sampled a target area west of Svalbard, including the marginal sea ice zone (Fig. 1b). The research aircraft HALO allowed to follow air masses over several consecutive days to study their development over a larger time range. In contrast, Polar 5 and Polar 6 have the ability to study cloud micro- and macrophysics in more detail due to their slower cruising speed and lower altitudes. Therefore, the combination of the measurements from HALO and the Polar aircraft gives the unique opportunity to study the development of air masses, i.e., WAIs and CAOs, on large and small scales. A more detailed overview about the conducted flights is given in Table 1, which shows for each flight the objective, flight time and the launched number of dropsondes. For

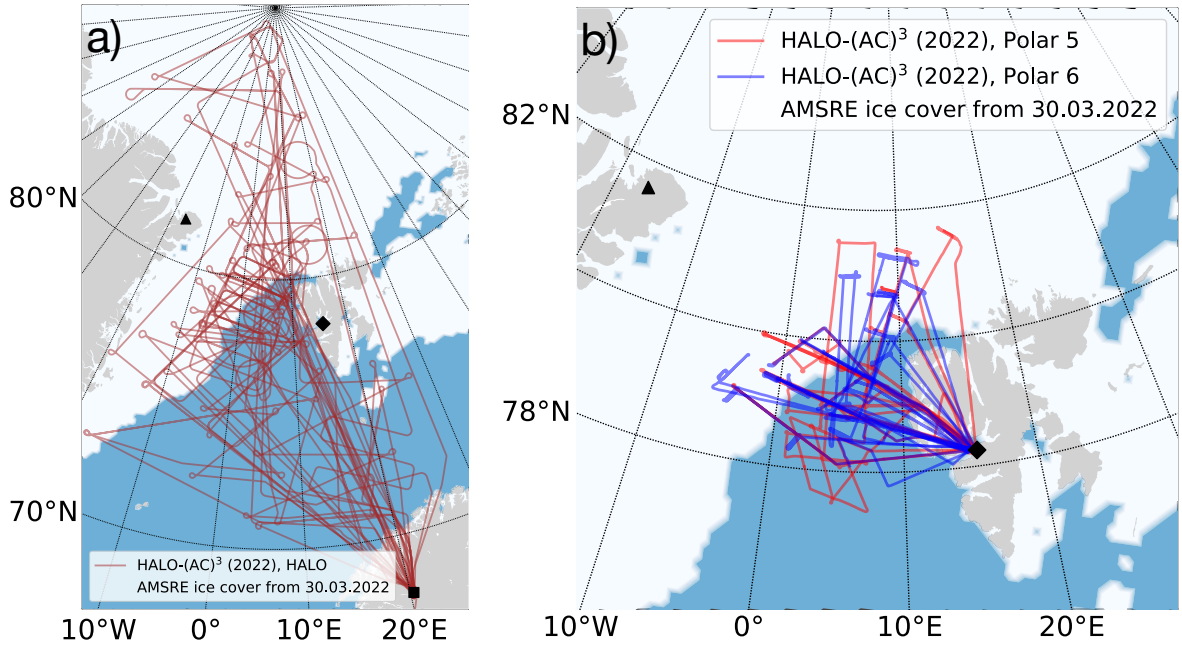


Figure 1: *Flight tracks of the HALO-(AC)$^3$ campaign from a) the research aircraft HALO and b) Polar 5 (red) and Polar 6 (blue). The black markers indicate the location of Station North (triangle), Longyearbyen (diamond) and Kiruna (square).*

the whole campaign we spend more than 264 hours in the air (HALO: 147 h, Polar 5: 54 h, Polar 6: 63 h). In total 492 dropsondes were launched, which provided valuable atmospheric profile data without technical issues in more than 95 % .

In the following we will give an overview of research projects at LIM, which are linked to HALO-(AC)$^3$ and make use of the airborne observations. Section 2 is focusing on atmospheric vertical profiles, which were observed by dropsondes launched over sea-ice and ice-free ocean. Section 3 shows an example of a collocated flight from Polar 5 and Polar 6. In Sect. 4 a Lagrangian trajectory analysis of a WAI is presented, followed by a summary of the results.

## 2 Vertical profiles of the atmosphere

During the HALO-(AC)$^3$ campaign, 350 dropsondes were launched from the HALO and 142 from the Polar 5 aircraft. This large amount of dropsondes is statistically applied to identify the typical differences of vertical profiles over the Arctic sea-ice and ice-free ocean. Therefore, we analysed all dropsondes launched from HALO poleward of 75°N. This threshold was chosen to only compare the atmosphere in the vicinity of the marginal sea ice zone.

The separated profiles over sea-ice and ice-free ocean are shown in Fig. 2. It is obvious that over sea-ice the atmosphere shows in general a lower temperature below 2000 m (Fig. 2a and b) and is also dryer (Fig. 2c). As shown in Fig. 2d, the wind speed throughout the whole vertical profile is lower over ice than over the ice-free ocean and is affected by the friction from the ground. Above sea ice, a temperature inversion is visible in an altitude below 1000 m (Fig. 2a), which is very typical over sea-ice. The

| Date | Flight # | HALO Objective | Duration | Dropsondes | Flight # | Polar 5 Objective | Duration | Dropsondes | Flight # | Polar 6 Objective | Duration |
|---|---|---|---|---|---|---|---|---|---|---|---|
| **25 February 2022** | **0** | Scientific test flight | 04:41 | 2 | | | | | | | |
| **10 March 2022** | | | | | **0** | Scientific test flight | 02:00 | | | | |
| **11 March 2022** | **1** | Transfer to Kiruna | 03:03 | | | | | | | | |
| **12 March 2022** | **2** | Warm air intrusion #1, Day 1 | 08:22 | 20 | | | | | | | |
| **13 March 2022** | **3** | Warm air intrusion #1, Day 2 | 08:48 | 23 (2 failed) | | | | | | | |
| **14 March 2022** | **4** | Warm air intrusion #1, Day 3 | 08:33 | 11 (1 failed) | | | | | | | |
| **15 March 2022** | **5** | Atmospheric river #1, Day 1 | 08:42 | 25 | | | | | | | |
| **16 March 2022** | **6** | Atmospheric river #1, Day 2 | 09:29 | 25 (2 failed) | | | | | | | |
| **20 March 2022** | **7** | Day before cold air outbreak #1 | 09:08 | 18 (1 failed) | **1** | P5 & P6 collocation over sea ice and ocean | 04:12 | 12 | **1** | Low level clouds & aerosol | 04:40 |
| **21 March 2022** | **8** | Coordination with in-situ meas. by FAAM | 07:47 | 13 | | | | | | | |
| **22 March 2022** | | | | | **2** | CAO #1 | 01:35 | 2 | **2** | In-situ cloud & aerosol | 05:30 |
| | | | | | **3** | CAO #1 | 04:15 | 10 | | | |
| **24 March 2022** | | | | | | | | | **3** | In-situ cloud & aerosol | 05:24 |
| **25 March 2022** | | | | | **4** | Boundary layer flight over MIZ | 04:56 | 4 | | | |
| **26 March 2022** | | | | | | | | | **4** | Low level clouds of CAO | 04:00 |
| **28 March 2022** | **9** | CAO #2 | 07:27 | 22 (6 failed) | **5** | Cloud streets in Svalbard lee | 04:35 | 15 | **5** | Moderate CAO and cloud streets | 04:50 |
| **29 March 2022** | **10** | Coordination east of Svalbard with FAAM | 08:24 | 18 | **6** | Test of noseboom | 01:01 | | **6** | Stack profile patterns | 05:28 |
| | | | | | **7** | Boundary layer flight over sea ice and open ocean | 05:10 | 5 | | | |
| **30 March 2022** | **11** | CAO #2, Divergence circles | 08:24 | 32 | **8** | Weak outflow of CAO | 04:23 | 15 | **7** | Racetrack pattern in vicinity of HALO track | 05:00 |
| **01 April 2022** | **12** | CAO #2, Rectangular divergence pattern | 08:11 | 45 (5 failed) | **9** | Different stages of cloud streets with P6 and HALO | 05:02 | 18 | **8** | Coordinated flights with P5 and HALO | 05:13 |
| **03 April 2022** | | | | | | | | | | | |
| **04 April 2022** | **13** | CAO #2, collocated flights | 08:52 | 13 | **10** | CAO and convergence | 04:16 | 14 | **9** | Clouds over open water | 04:20 |
| **05 April 2022** | | | | | **11** | Wing-by-wing and collocation with P6 | 04:20 | 10 | **10** | Wing-by-wing and collocation with P6 | 04:30 |
| **07 April 2022** | **14** | Arctic cirrus #1, collocated flights | 07:45 | 16 | **12** | Upper cirrus over low level clouds | 04:23 | 18 | | | |
| **08 April 2022** | **15** | Polar low | 07:19 | 21 | | | | | **11** | Clouds in vicinity of polar low | 05:15 |
| **09 April 2022** | | | | | | | | | **12** | Boundary layer measurements | 04:48 |
| **10 April 2022** | **16** | Arctic cirrus #2, Day 1 | 06:30 | 22 | **13** | Low level clouds over sea ice and open ocean | 04:56 | 19 (1 failed) | **13** | Cloud measurements ove ice and open ocean | 04:58 |
| **11 April 2022** | **17** | Arctic cirrus #2, Day 2 | 07:55 | 7 | | | | | | | |
| **12 April 2022** | **18** | Arctic cirrus #2, Day 3 | 08:06 | 17 | | | | | | | |
| **Total:** | | | **147:26** | **350 (17 failed)** | | | **54:08** | **142 (1 failed)** | | | **63:56** |

Table 1: *Overview of the research flights of the HALO, Polar 5, and Polar 6 during HALO-(AC)*$^3$.

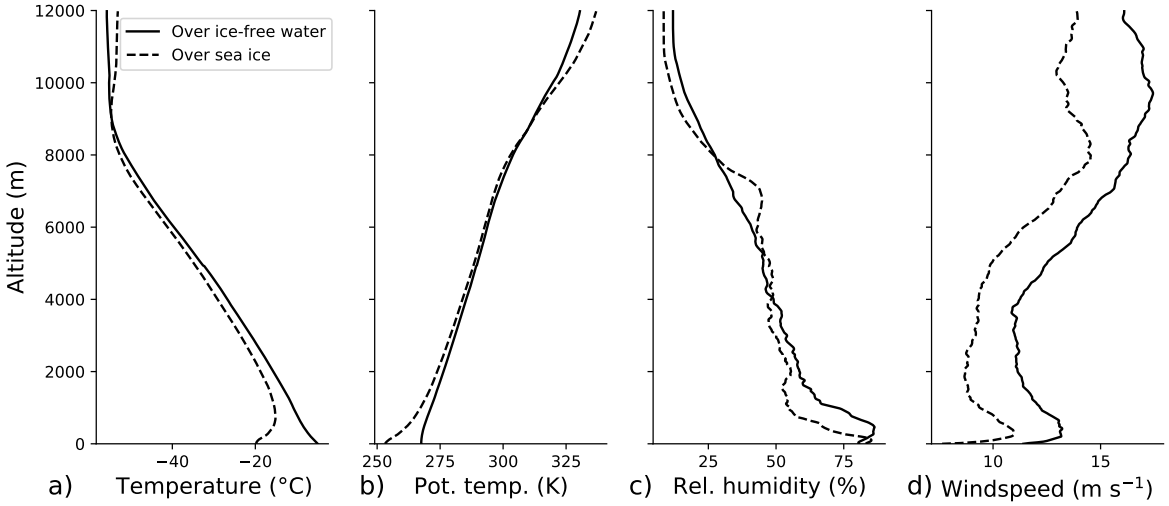


Figure 2: *Averaged dropsonde profiles, launched from HALO, over Arctic sea ice (dashed) and over ice-free ocean during HALO-(AC)*$^3$*. Only dropsondes launched poleward of 75°N are displayed here, which results in 122 dropsondes over ice-free ocean and 109 over sea-ice.*

relative humidity profiles indicate that less clouds were observed over sea ice (Fig. 2c).

### 2.1 Profiles along a cold air outbreak

Marine CAOs are very common in the Arctic winter time and can influence the weather in Europe. The CAOs can often be easily identified by their typical roll cloud structure, which is visible from satellite images. In the vicinity of Svalbard, in particular on the west side, CAOs are very typical with a north-south wind direction (Brümmer, 1996; Dahlke et al., 2022). Usually, the roll clouds develop over the marginal sea ice zone with an increasing cloud top height towards the south. The development process of the roll clouds is related to the increased temperature and moisture over the ice-free ocean. Towards the south, the surface temperature increases, which strengthens the convection and increases the cloud top height. The change in cloud top height also influences the horizontal size of the roll clouds, because the distance between the rolls depends on the cloud top height and the ratio is about 2:1 (Lemone, 1976). Roll clouds in connection with CAOs were extensively studied before (Kuettner, 1971; Lemone, 1976; Brümmer, 1996; Tornow et al., 2022; Dahlke et al., 2022), but covering a CAO event with different aircraft on a small (with Polar 5 and Polar 6) and large (with HALO) scale is new and gives a whole new insight of the development of these air masses.

The development of atmospheric vertical profiles along a CAO is presented in Fig. 3. This CAO case was observed on 01 April 2022. Illustrated by the flight track in Fig. 3a, the HALO aircraft covers a majority of the roll cloud structures starting from the beginning until almost the end of their development. Along that path, several dropsondes were launched. Here, we focus on the dropsonde profiles at the eastern leg of the flight track along the roll convection (marked by the dots in Fig. 3). Figures 3b and c show profiles of temperature and potential temperature, respectively, of the developing CAO and indicate the typical increase of temperature from north to south. The increase in cloud top height

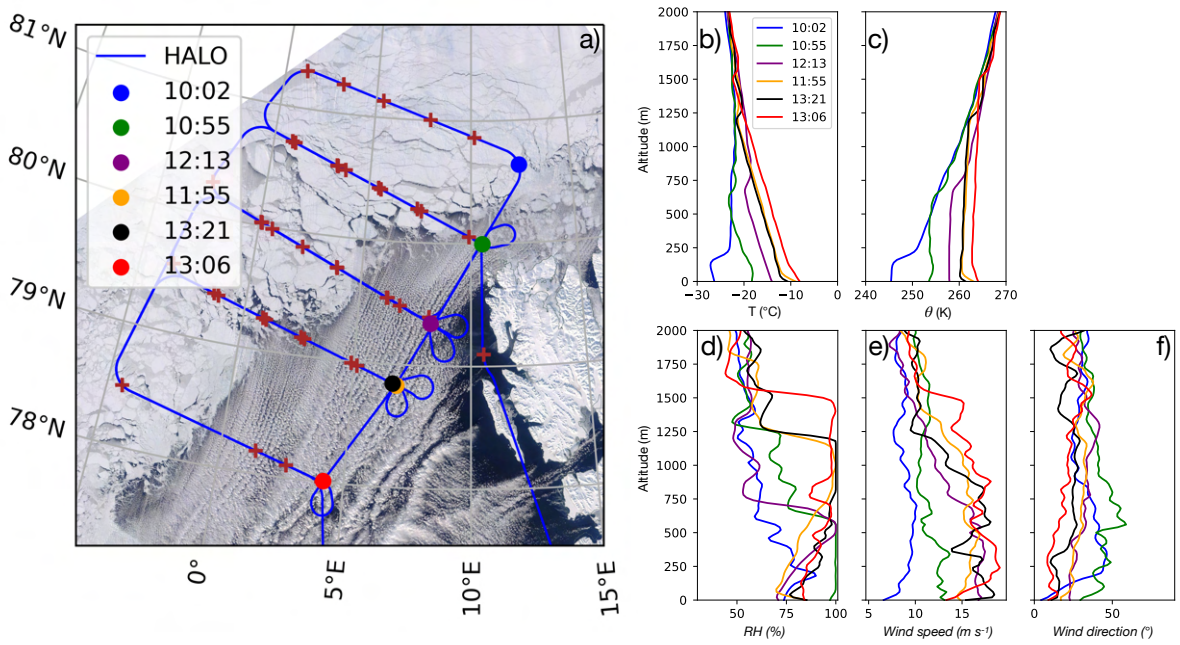


Figure 3: *a) HALO flight track from the 01 April 2022 in the vicinity of Svalbard. The crosses mark the positions of the launched dropsondes and the satellite picture is a snapshot from NASA worldview (MODIS). The dots indicate the dropsondes where the vertical profiles of different parameters are shown in panels b to f.*

is linked to the change of inversion height from about 100 m (blue point over ice) to about 1500 m (red point over water). That almost no clouds are present over the Arctic sea-ice is concluded from the relative humidity profiles in Fig. 3d. Here, a relative humidity of 100 %, which means the presence of clouds, is only reached over water and not for the profile over sea ice (blue). The wind speed (see Fig. 3e) shows an increase towards the south, which is contrarily to CAOs observed in earlier campaigns. Typically, the wind speed is highest above the ice where surface friction is low. Wind direction (see Fig. 3f) is in a narrow range for all profiles, which confirms a very steady air mass flow from the north. It might be noted that the dropsondes at 11:55 UTC and 13:21 UTC were launched at a very similar position. This was done to examine the temporal consistency of the dropsonde profiles. It turns out that the profiles are very consistent, in particular for the temperature, even though the measurements were taken 86 minutes apart.

This analysis shows that dropsonde measurements can be used to study the development of CAOs. This is a first step to obtain a better understanding of the development process of CAOs. Including radar reflectivity data from the Microwave Radar/radiometer for Acrtic Clouds (MiRAC) instrument (Mech et al., 2019) and radiance data from the Spectral Modular Airborne Radiation measurement sysTem (SMART) instrument (Wendisch et al., 2001) in the analysis, both on board of Polar 5, we will obtain more information about the distribution of ice and liquid water in the roll clouds.

## 3 Collocated research flights

A major goal of the HALO-(AC)$^3$ campaign was the collocation of measurements from different aircraft, in particular from Polar 5 and Polar 6. Performing remote-sensing

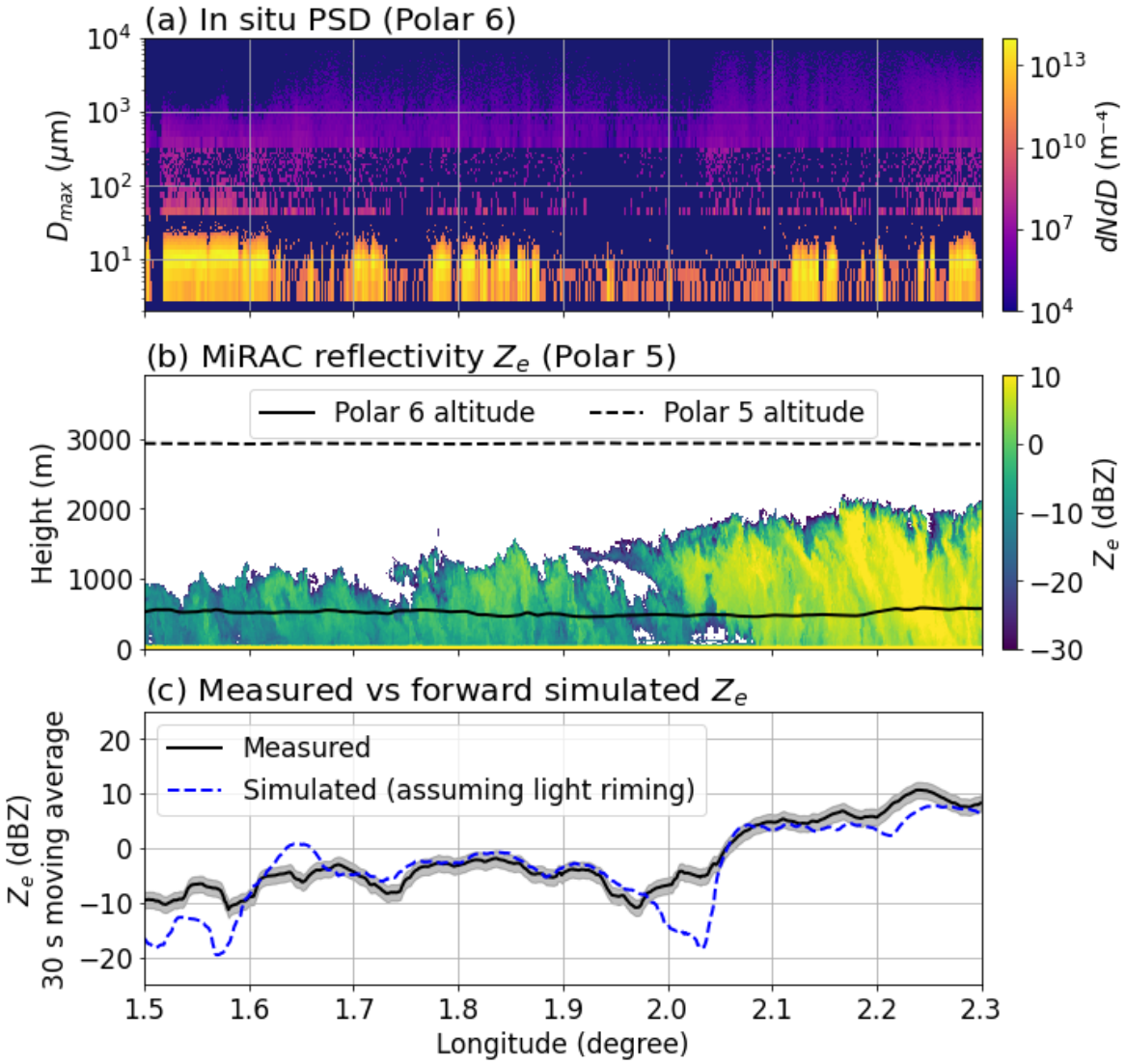


Figure 4: *Collocated flight between Polar 5 and Polar 6 for a flight segment of 12 minutes on 28 March 2022, between 14:12:30 and 14:14:20 UTC. a) in-situ particle size distributions (PSD), recorded with different instruments on the Polar 6 aircraft. b) MiRAC radar reflectivity measurements taken from the Polar 5 aircraft. The horizontal lines represent the altitude from the two Polar research aircraft. c) Measured (MiRAC) and simulated (PAMTRA) radar reflectivity for the flight altitude of the Polar 6.*

observations with Polar 5 and in-situ measurements with Polar 6 is used to characterize cloud micro- and macrophysical properties. These collocated data set is very valuable for the development of cloud retrieval algorithms. During the HALO-(AC)$^3$ campaign both Polar aircraft spent in total 13 hours and 17 minutes, in a spatial range of 10 km and a temporal range of 5 minutes, together. A section of these collocated measurements is displayed in Fig. 4. The measurements from 28 March 2022 show a size distribution of in-situ particle measurements, operated on Polar 6 (Fig. 4a) and radar reflectivity measurements from the MiRAC instrument (Mech et al., 2019) on Polar 5 (Fig. 4b). Based on the in-situ particle measurements, forward simulations were made with the Passive and Active Microwave TRAnsfer (PAMTRA) tool (Mech et al., 2020), assuming light riming. The result of the simulations is shown in Fig. 4c and compared to the

measured radar reflectivity. In general there is a good agreement, just below 1.6° and around 2.0° longitude the simulations are clearly below the measured radar reflectivity, which indicates a stronger riming of the particles at these locations. The analysis of this flight section demonstrates that it is possible to derive the radar reflectivity from in situ particle size distributions. In a future study we aim to invert the radar measurements and use similar tools to derive the cloud particle properties from remote sensing. This will be more challenging, because the PSD and the amount of riming is unknown.

## 4 Lagrangian trajectory analysis of a Warm Air Intrusion

The meteorological state in the Arctic was analyzed based on ERA5 reanalysis data (Hersbach et al., 2020). Many atmospheric observations collected during the campaign, such as most dropsonde thermodynamics profiles, were directly assimilated into ERA5. Furthermore, ERA5 has been shown to outperform several other reanalyses in Fram Strait (Graham et al., 2019a,b). For trajectory calculations, ERA5 wind fields were used in conjunction with the *Lagranto* analysis tool (Sprenger and Wernli, 2015). For the analysis presented here, trajectories were started:

- Temporally, every full hour between 9-15 March 2022
- Horizontally, along the 80°N latitude circle, in 1° steps between 15°W to 10°E (i.e., between Greenland and Svalbard)
- Vertically, at a pressure level of 850 hPa

Trajectories were calculated 60 hours (2.5 days) forward in time. Along the trajectories, a set of meteorological parameters were extracted from ERA5. In particular, the analysis aimed at:

- The normalized density of trajectories per 100 $km^2$ area
- The air mass properties at the start of the drift, i.e., in Fram Strait
- The total change in meteorological parameters, i.e., the end value (t = +60 hours) minus the start value (t = 0 hours)

### 4.1 Synoptic conditions and air mass pathways

Figure 5 shows the ERA5-derived synoptic conditions for two distinct periods in mid-March 2022. The period 9-11 March 2022 was defined as background period, as here no increased values for total column water vapor were detected in the central Arctic. On the contrary, 12-15 March 2022 was defined as WAI period. Driven by a dipole pattern in mean sea-level pressure (black isobars), large amounts of water vapor (upper row) and heat (lower row, air temperature at 850 hPa altitude) were advected towards the North Pole. In the following chapter, the differences between these two periods are characterized.

Figure 6 depicts the normalized density of air masses on their 2.5-day drift, starting in Fram Strait. As can be seen, two very separate pathways emerge for the two time

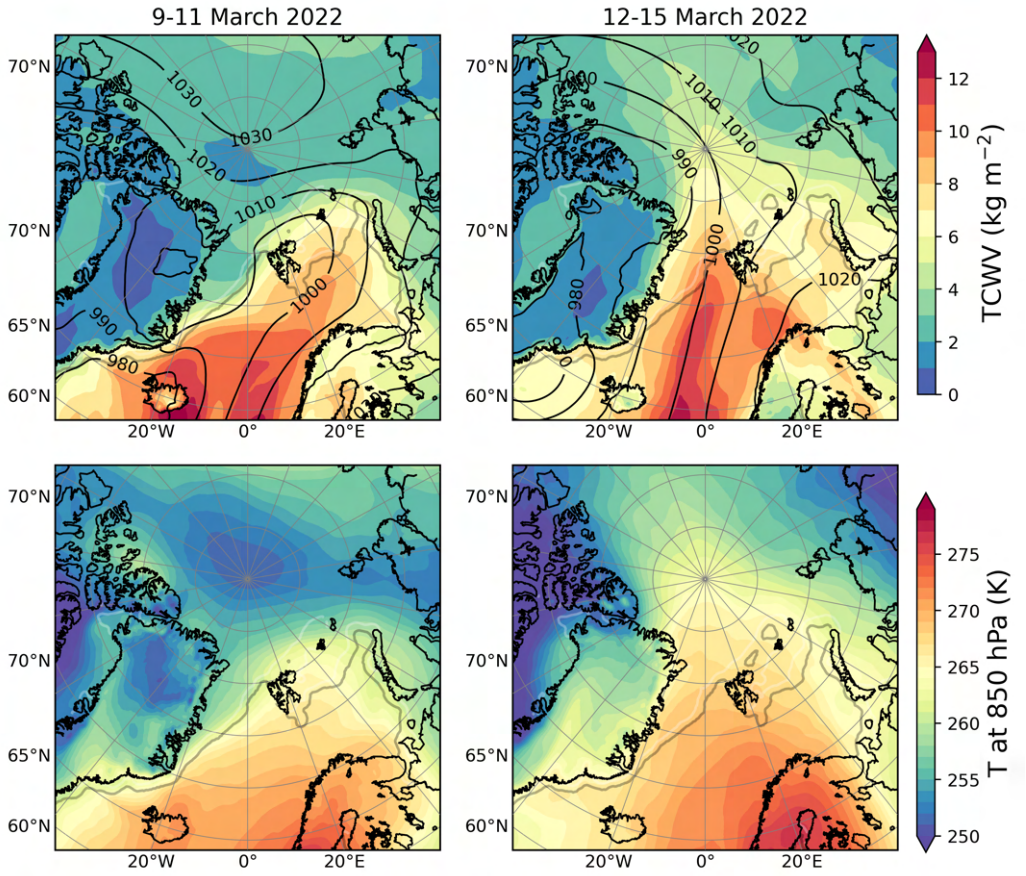


Figure 5: *Synoptic overview of the two periods, based on ERA5. Depicted are the mean values of (top panel) total column water vapor (filled contours), mean sea-level pressure (contours, in hPa), (bottom panel) air temperature at the 850 hPa pressure level. In all graphs, the gray lines denote the 15 % and 80 % sea-ice margins.*

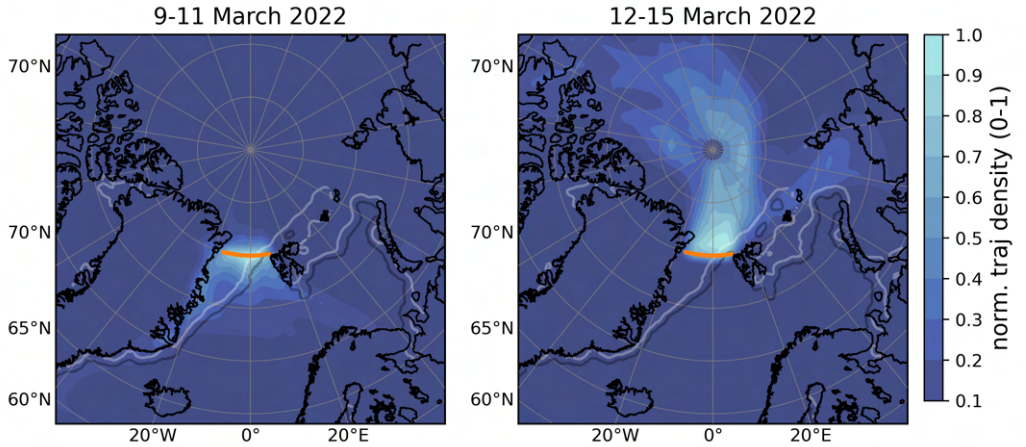


Figure 6: *Normalized density of air mass trajectories initiated at 850 hPa altitude in Fram Strait (orange line) along their 2.5-day drift. Two distinct periods are contrasted, 9-11 March 2022 versus 12-15 March 2022. The gray lines denote the 15 % and 80 % sea-ice margins. Data is based on ERA5 wind fields and Lagranto.*

periods. During 9-11 March 2022 air masses mostly drifted very slowly and generally southwards. On the contrary, 12-15 March 2022 air masses were strongly pushed northwards and traversed the North Pole.

These two pathways were not only geographically different, the properties of air masses at the start and along the flow were also different.

### 4.2 Properties along pathways

Figures 7a and b compare the frequency distribution of the potential temperature $\theta$ and specific humidity $q$ of the two air masses at the start of the trajectories. The change of both parameters along the air mass trajectory is presented in Fig. 7c and d. At the starting location, the background period of 9-11 March 2022 was characterized by an air mass with a mean 850 hPa potential temperature of around 270 K, and on average very low specific humidities of about 1 g kg$^{-1}$. On their 2.5-day drift, the air mass generally underwent medium moistening by 0-2 g kg$^{-1}$. The distribution of potential temperature change was bimodal. One mode was centered around 0 K, i.e., air masses moved isentropically and did not undergo excessive heating. The slightly weaker second mode peaked at an average diabatic warming of about 7 K. Overall, the 9-11 March 2022 air parcels showed many properties, which hinted towards a weak CAO, i.e., slight moistening and diabatic heating, possibly reinforced by surface sensible and latent heat fluxes from the warm ocean. This is in line with the trajectories depicted in Fig. 6.

In contrast, the WAI during 12-15 March 2022 caused a different transition of the air mass. Already at the start location, potential temperatures were about 10 K higher, at around 280 K. Furthermore, most air masses had an initial specific humidity of more than 3 g kg$^{-1}$. On their path towards the North Pole, these air masses lost most of their

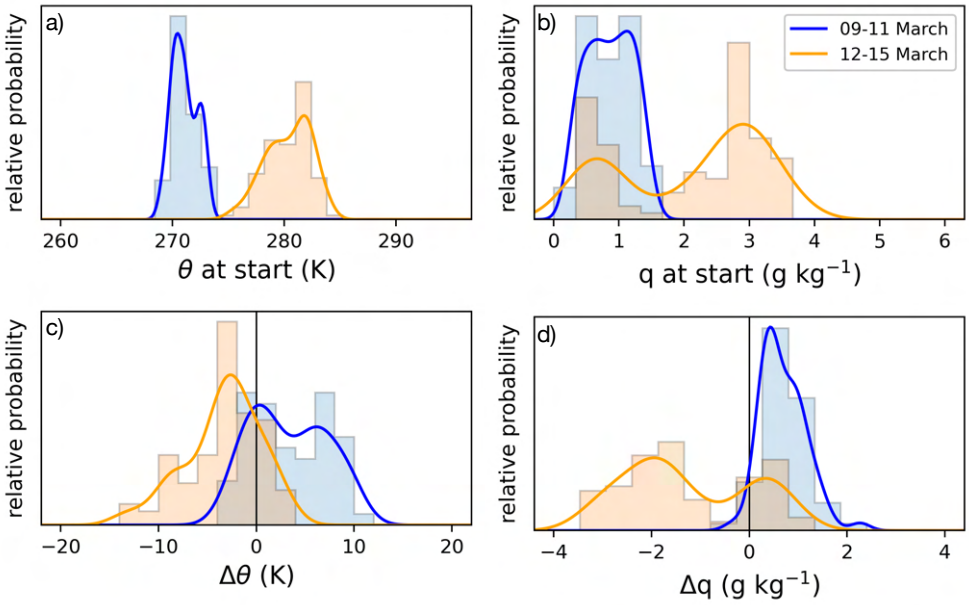


Figure 7: *Comparison of different air mass properties at the start and during their 2.5-day drift. Shown are the histograms and kernel density functions for 9-11 March 2022 in contrast to 12-15 March 2022. The parameters comprise a) potential temperature θ and b) specific humidity q at start, as well as their total change within 2.5 days (c and d).*

water vapor. Not least to their high initial air temperatures, they also cooled diabatically, with mean values of -3 K to -8 K in 2.5 days.

## 5 Summary and conclusions

In this report, we summarized the current activities of LIM with respect to the airborne observations of Arctic air mass transformations during the HALO-(AC)$^3$ mission. The campaign was conducted in March and April 2022 with the goal to perform quasi-Lagrange observations of air mass transformations and to test the ability of numerical atmospheric models to reproduce the measurements. Three aircraft, namely HALO, Polar 5 and Polar 6, were involved to study clouds and the Arctic atmosphere on large and small spatial scales. Three studies using HALO-(AC)$^3$ observations and reanalysis data that are lead by LIM are reported here.

Vertical profiles characterizing the Arctic atmosphere are analyzed. With 492 launched dropsondes, the Arctic atmosphere was extensively probed during HALO-(AC)$^3$. Vertical profiles of atmospheric properties were compared for locations over sea-ice and the ice-free ocean. The comparison shows that in general lower temperatures, lower relative humidities and lower wind speeds were present over ice than over ice-free ocean. In addition, dropsonde profiles were analyzed along a CAO and show how the warm ocean surface affects the air mass transformation.

Collocated observations from Polar 5 and Polar 6 were analyzed. In particular, radar reflectivities were simulated based on in-situ measurements of cloud particle properties measured with the Polar 6 aircraft. To evaluate how accurate these simulations are, the results were compared with the radar measurements from the Polar 5 aircraft. This comparison shows a good agreement between radar reflectivity measurements and simulations based on in-situ measurements indicating the potential of the collocated data set.

Lagrangian trajectory analysis were used to characterize the synoptic conditions during mid-March 2022, i.e., at the start of the HALO-(AC)$^3$ airborne campaign. The background period defined here as 9-11 March 2022 was compared to the WAI period of 12-15 March 2022. Two distinct pathways of air masses were found for these periods. While the background case showed a slow southward drift of Fram Strait air parcels, the WAI pushed large amounts of air towards the North Pole and beyond. The analysis of air mass properties along their trajectories showed that not only the air-mass properties at the start in Fram Strait differed, but also thermodynamic processes along the flow (diabatic heating/cooling, moisture changes). It can be concluded that air masses in the two periods underwent clearly distinct transformation processes.

These examples indicate the potential of the observations during the HALO-(AC)$^3$ mission. Future analyis of the data will aim at a better understanding of how the transport of air masses in the Arctic works and how it affects the large-scale environment.

## Acknowledgements

We gratefully acknowledge the funding by the Deutsche Forschungsgemeinschaft (DFG, German Research Foundation) – Project Number 268020496 5 – TRR 172, within the

Transregional Collaborative Research Center "ArctiC Amplification: Climate Relevant Atmospheric and SurfaCe Processes, and Feedback Mechanisms $(AC)^3$.

## References


Brümmer, B.: Boundary-layer modification in wintertime cold-air outbreaks from the Arctic sea ice, Boundary-Layer Meteorology, 80, 109–125, doi:10.1007/BF00119014, 1996.

Dahlke, S., Solbès, A., and Maturilli, M.: Cold Air Outbreaks in Fram Strait: Climatology, Trends, and Observations During an Extreme Season in 2020, Journal of Geophysical Research: Atmospheres, 127, doi:10.1029/2021JD035741, 2022.

Graham, R., Cohen, L., Ritzhaupt, N., et al.: Evaluation of six atmospheric reanalyses over Arctic sea ice from winter to early summer, J. Clim., 32, 4121–4143, doi:10.1175/JCLI-D-18-0643.1, 2019a.

Graham, R. M., Itkin, P., Meyer, A., et al.: Winter storms accelerate the demise of Arctic sea ice, Sci. Rep., 9, 9222, doi:10.1038/s41598-019-45574-5, 2019b.

HALO-$(AC)^3$ Website: HALO-$(AC)^3$ - Arctic Air Mass Transformations During Warm Air Intrusions and Marine Cold Air Outbreaks, URL `https://halo-ac3.de/halo-ac3/campaign/`, 2023.

Hersbach, H., Bell, B., Berrisford, P., et al.: The ERA5 global reanalysis, Quarterly Journal of the Royal Meteorological Society, 146, 1999–2049, doi:10.1002/qj.3803, 2020.

Kuettner, J. P.: Cloud bands in the earth's atmosphere: Observations and Theory, Tellus, 23, 404–426, doi:10.1111/j.2153-3490.1971.tb00585.x, 1971.

Lemone, M. A.: Modulation of turbulence energy by longitudinal rolls in an unstable planetary boundary layer, Journal of the Atmospheric Sciences, 33, 1308–1320, 1976.

Mech, M., Kliesch, L.-L., Anhäuser, A., et al.: Microwave Radar/radiometer for Arctic Clouds (MiRAC): first insights from the ACLOUD campaign, Atmospheric Measurement Techniques, 12, 5019–5037, doi:10.5194/amt-12-5019-2019, 2019.

Mech, M., Maahn, M., Kneifel, S., et al.: PAMTRA 1.0: the Passive and Active Microwave radiative TRAnsfer tool for simulating radiometer and radar measurements of the cloudy atmosphere, Geoscientific Model Development, 13, 4229–4251, doi:10.5194/gmd-13-4229-2020, 2020.

Rantanen, M., Karpechko, A. Y., Lipponen, A., et al.: The Arctic has warmed nearly four times faster than the globe since 1979, Communications Earth & Environment, 3, 168, doi:10.1038/s43247-022-00498-3, 2022.

Serreze, M. C. and Barry, R. G.: Processes and impacts of Arctic amplification: A research synthesis, Global and Planetary Change, 77, 85–96, doi:10.1016/j.gloplacha.2011.03.004, 2011.

Sprenger, M. and Wernli, H.: The Lagrangian analysis tool LAGRANTO – version 2.0, Geosci. Model Dev. Discuss., 8, 1893–1943, doi:10.5194/gmdd-8-1893-2015, 2015.

Tornow, F., Ackerman, A. S., Fridlind, A. M., et al.: Dilution of Boundary Layer Cloud Condensation Nucleus Concentrations by Free Tropospheric Entrainment During Marine Cold Air Outbreaks, Geophysical Research Letters, 49, e2022GL098 444, doi:10.1029/2022GL098444, e2022GL098444 2022GL098444, 2022.

Wendisch, M., Müller, D., Schell, D., and Heintzenberg, J.: An Airborne Spectral Albedometer with Active Horizontal Stabilization, Journal of Atmospheric and Oceanic Technology, 18, 1856 – 1866, doi:10.1175/1520-0426(2001)018<1856:AASAWA>2.0.CO;2, 2001.

Wendisch, M., Brückner, M., Crewell, S., et al.: Atmospheric and Surface Processes, and Feedback Mechanisms Determining Arctic Amplification: A Review of First Results and Prospects of the (AC)3 Project, Bulletin of the American Meteorological Society, 104, E208 – E242, doi:10.1175/BAMS-D-21-0218.1, 2023.

Wesche, C., Steinhage, D., and Nixdorf, U.: Polar aircraft Polar5 and Polar6 operated by the Alfred Wegener Institute, Journal of large-scale research facilities Facilities, 2, doi:10.17815/jlsrf-2-153, 2016.